Supporting information

Rational Surface Engineering of MXene@N-doping Hollow Carbon Dual-confined Cobalt Sulfides/Selenides for Advanced Aluminum Batteries

Long Yao, Shunlong Ju, Xuebin Yu*

Department of Materials Science, Fudan University, Shanghai 200433, China
E-mail: yuxuebin@fudan.edu.cn

Experimental section

Synthesis of Delaminated $Ti_3C_2T_x$ MXene

First, 1.0 g of LiF (Sigma Aldrich) was added into 20 mL of 9 M HCl (Sigma Aldrich), and the solution was stirred for 5 min. Then, 1 g of Ti_3AlC_2 MAX phase powder was slowly added to the solution and kept at 35 °C for 24 h under constant stirring. After that, the mixture was washed with deionized water for several times, until the supernatant reached a pH of approximately 6. The precipitates were then ultrasonicated in an ice-bath for 2 h. Finally, the supernatant was collected by centrifugation at 3500 rpm for 1h.

Preparation of ZIF-67@MXene and ZIF-67 Precursor

The ZIF-67@MXene composite was prepared by the coprecipitation. In detail, 5 mL of 0.206 mM cobalt nitrate aqueous solution with 6 mg PVP was sufficiently dissolved into 1 mL of 6 mg mL^{-1} MXene suspension. Then, 5 ml of 0.824 mM 2-methylimidazole aqueous solution with 200 ul triethylamine was added into above solution. After the mixture was incubated at room temperature for 4 h, the resulting purple precipitates were centrifuged and washed with deionized water for several times. To obtain the ZIF-67@MXene sponge-like precursor, the precipitates mixed with 1.5 mL deionized water were freeze dried for 48 h.

Synthesis of Co_9S_8 NP@NPC@MXene and Co_9S_8 NP@NPC

The Co_9S_8 NP@NPC@MXene was prepared by a simultaneous thermal-induced carbonization and sulfidation. Typically, ZIF-67@MXene precursor and appropriate S powder were put into a combustion boat and heated at rate of 2 ℃/min to 650℃ for 2h in flowing H_2/Ar (5/95, v/v) atmosphere. For comparison, Co_9S_8 NP@NPC composites were prepared through similar heat treatment using ZIF-67 as precursor.

Synthesis of $CoSe_2$@NPC@MXene and $CoSe_2$@NPC

Typically, ZIF-67@MXene precursor and appropriate Se powder were put into a combustion boat and heated at rate of 2 ℃/min to 650℃ for 2h in flowing H_2/Ar (5/95, v/v) atmosphere. For comparison, *$CoSe_2$@NPC* composites were prepared through similar heat treatment using ZIF-67 as precursor.

Preparation of the Ionic Liquid Electrolyte

The anhydrous $AlCl_3$ (99.999+%, Alfa Aesar) was slowly added to the dried 1-ethyl-3-methylimidazolium chloride ([EMIm]Cl, 98%, Alfa Aesar) ionic liquid with a molar ratio of 1.3:1 in an glovebox with O_2 < 0.1ppm and H_2O < 0.1ppm.

Material Characterization

The cobalt ion concentration was confirmed by ICP-MS (PerkinElmer NexION 300X). The crystalline structure of the products was investigated by XRD (Bruker D8 Advance, Cu Kα, λ = 0.151418 nm) from 5 to 80° with 10° min^{-1} steps. The morphologies and microstructures were examined by scanning electron microscope (SEM, 6390 and 6700F) and transmission electron microscope (TEM, JEOL 2010). The chemical states of the as-prepared active materials and electrodes after charge and discharge were identified by XPS (Thermo ESCALAB 250Xi, Al Kα

(hν = 1486.6 eV)). The BET specific surface area and pore size distributions were determined by N_2 adsorption-desorption isotherms at 77 K using a Trwastar-3020 instrument.

Electrochemical Measurement

The working electrodes were fabricated by mixing active materials, conductive carbon black, and the binder of sodium carboxymethyl cellulose at a mass ratio of 7:2:1. The mass loading of active materials in the electrode was around 0.8-1.0 mg cm^{-2}. The resultant paste was coated on the high pure Mo collector and the electrodes were dried at 80 °C under vacuum overnight. The swagelok-type cells were assembled with the high purity Al as the counter electrode, glass fiber (GF/D) as the separators, and as-prepared ionic liquid electrolytes as the electrolyte. The cells were set up in a glovebox filled with H_2O < 0.1 ppm and O_2 < 0.1 ppm. Galvanostatic charge/discharge measurements were carried out on a LAND battery test system (Wuhan, China). CV and EIS were conducted on a CHI 604E electrochemistry workstation.

Computational Details

The DFT calculation was performed using the Vienna ab initio Simulation Package, which uses the projector-enhanced wave approximation and the Perdew-Burke-Ernzerhof function to describe the exchange-related energy. A 520 eV cut-off value of the plane wave basis set was used to avoid Pulay stress, and the convergence criterion was set to 10^{-5} eV. Allow the position of the atoms to move until the force acting on each atom was < 0.02 eV/Å. The adsorption energy of atomic iodine on the 3×3 $Ti_3C_2T_x$ MXene supercell was calculated by selecting a k-point of 3×3×1. Applying a vacuum thickness of 15 Å can avoid the interaction between the slab and its periodic images. DFT-D3 correction was also used to account for van der Waals interaction.To evaluate the binding strength of Co on $Ti_3C_2T_x$ MXene, binding energy (E_b) was defined as

$$E_b = E_{Total} - E_{Co} - E_{Substrate}$$

where E_{Co} is the energy of single Co atom, E_{Total} and $E_{Substrate}$ are the calculated total energies of $Ti_3C_2T_x$ MXene with and without Co adsorbed, respectively. Charge density difference plots are obtained by subtracting the charge densities of pristine $Ti_3C_2T_x$ and isolated Co atom from that of Co adsorbed $Ti_3C_2T_x$. The yellow regions denote areas of charge accumulation while the blue regions denote charge depletion.

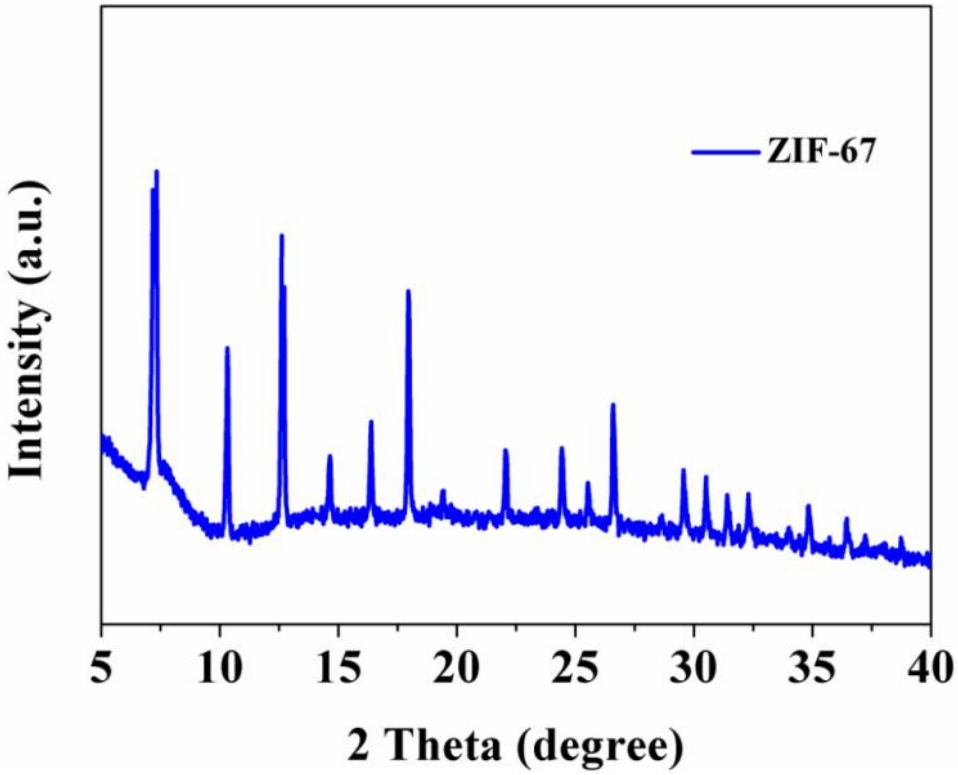

Fig. S1. XRD pattern of ZIF-67.

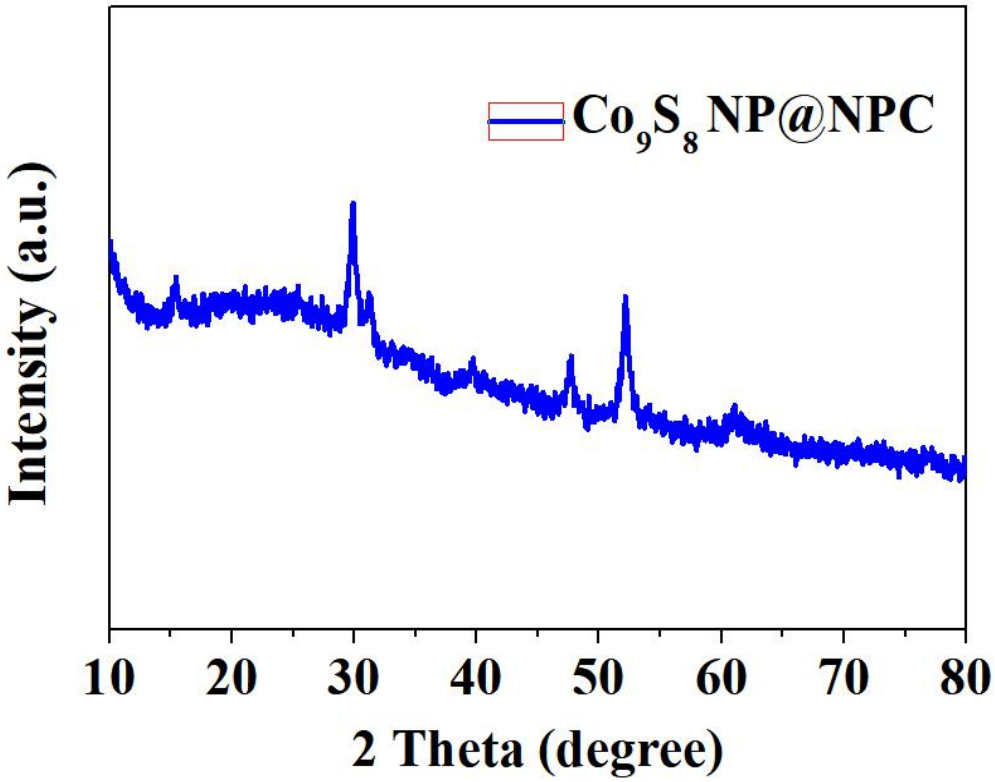

Fig. S2. XRD pattern of Co_9S_8 NP@NPC.

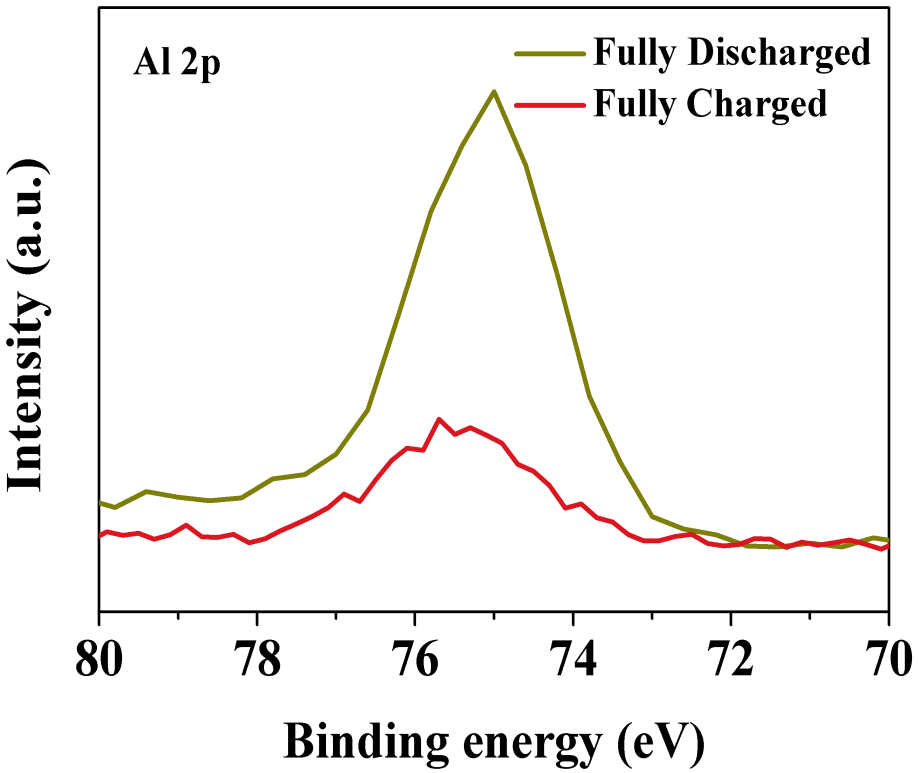

Fig. S3. XPS signals of Al 2p at various electrochemical states for Co_9S_8 NP@NPC electrode.

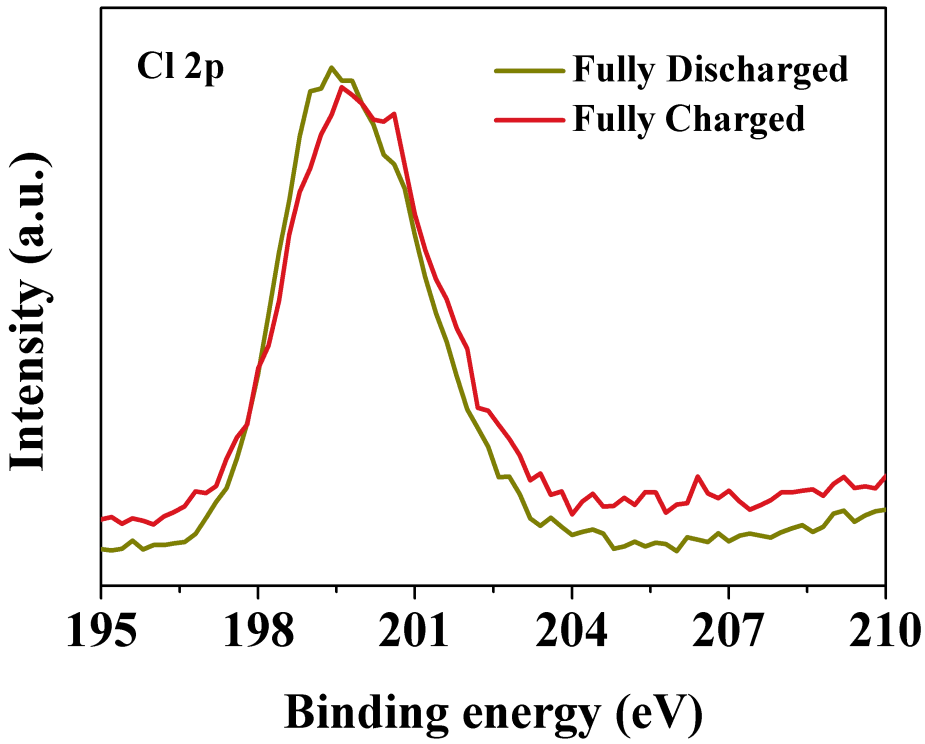

Fig. S4. XPS signals of Cl 2p at various electrochemical states for Co_9S_8 NP@NPC electrode.

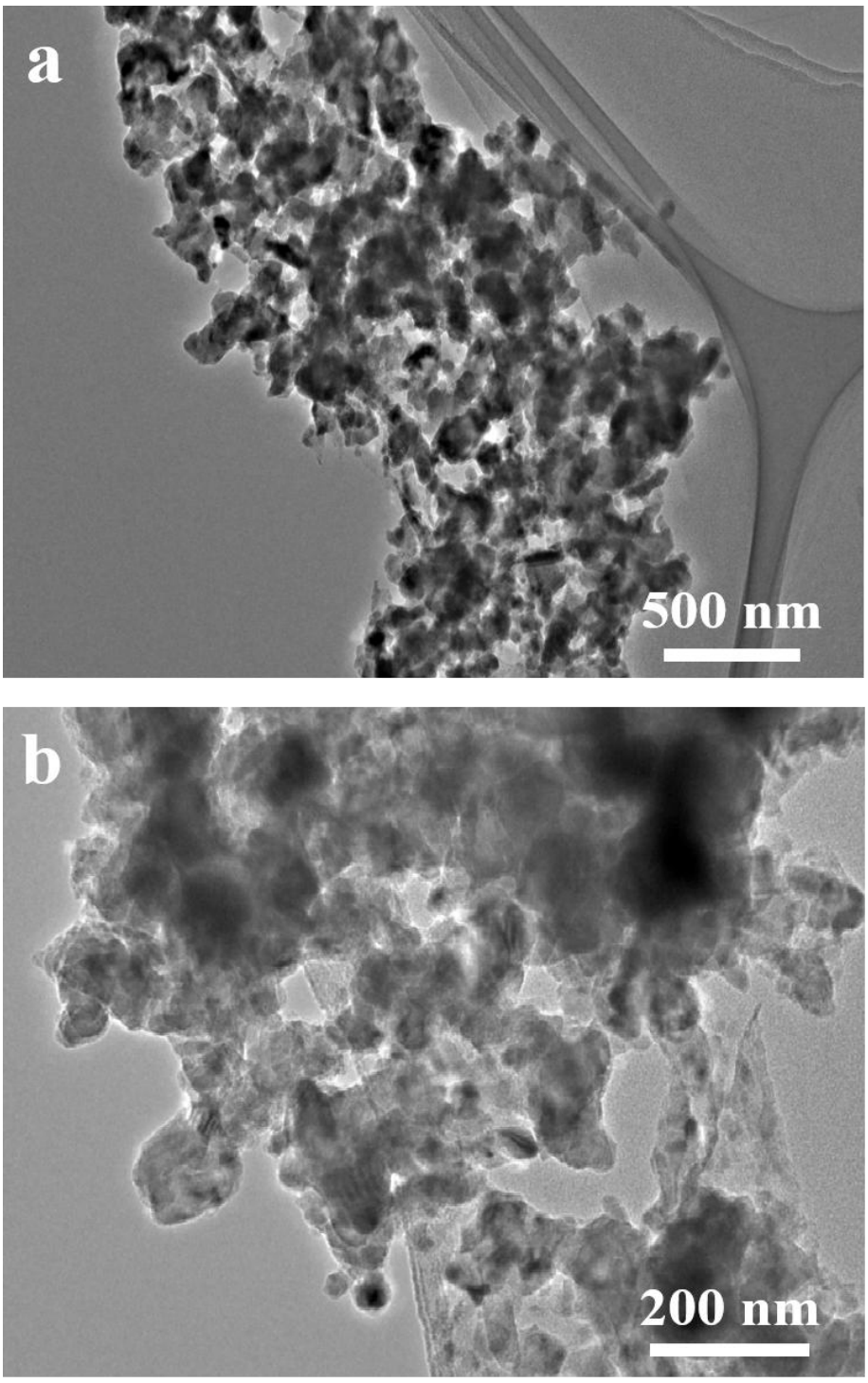

Fig. S5. (a,b) TEM images of the Co_9S_8 NP@NPC electrode after 100 cycles under different magnifications.

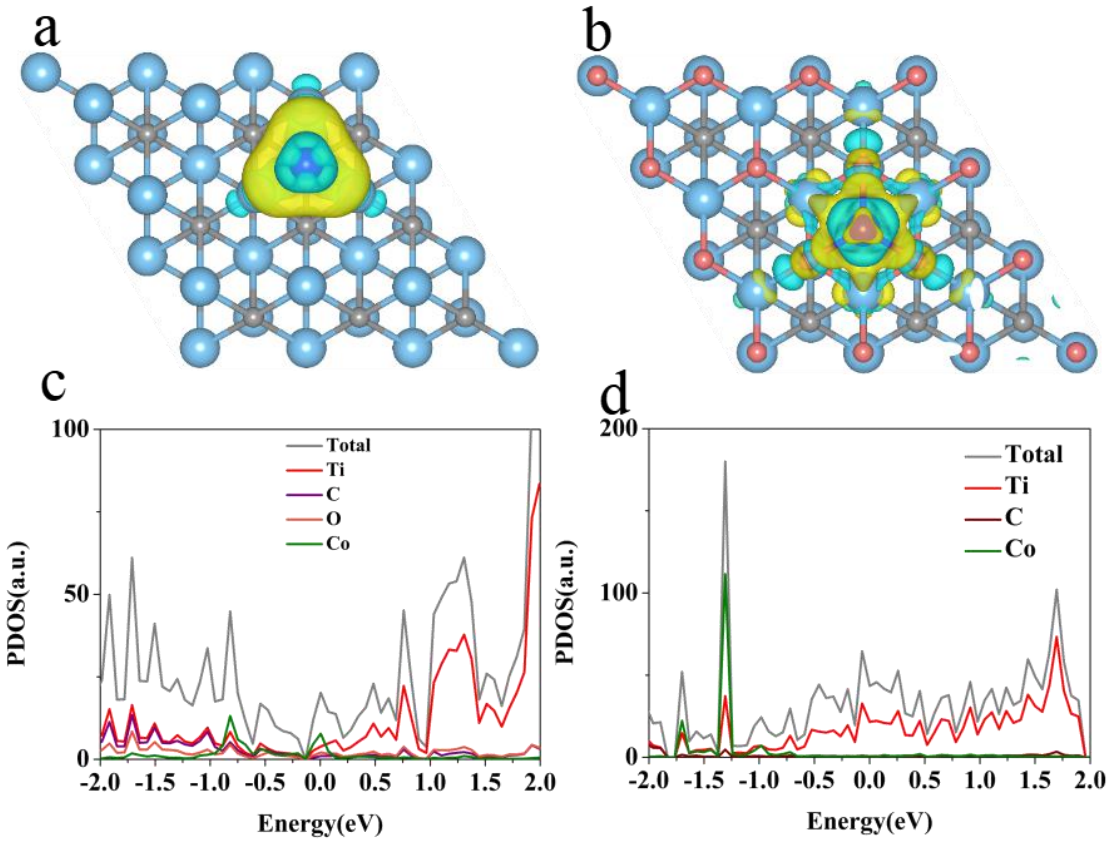

Fig.S6. (a) The charge density difference map calculations for MXene-Co;(b) the charge density difference map calculations for MXene-Co;(c) PDOS plots of MXene and adsorbed Co atom; (d) PDOS plots of MXene-O and adsorbed Co atom.

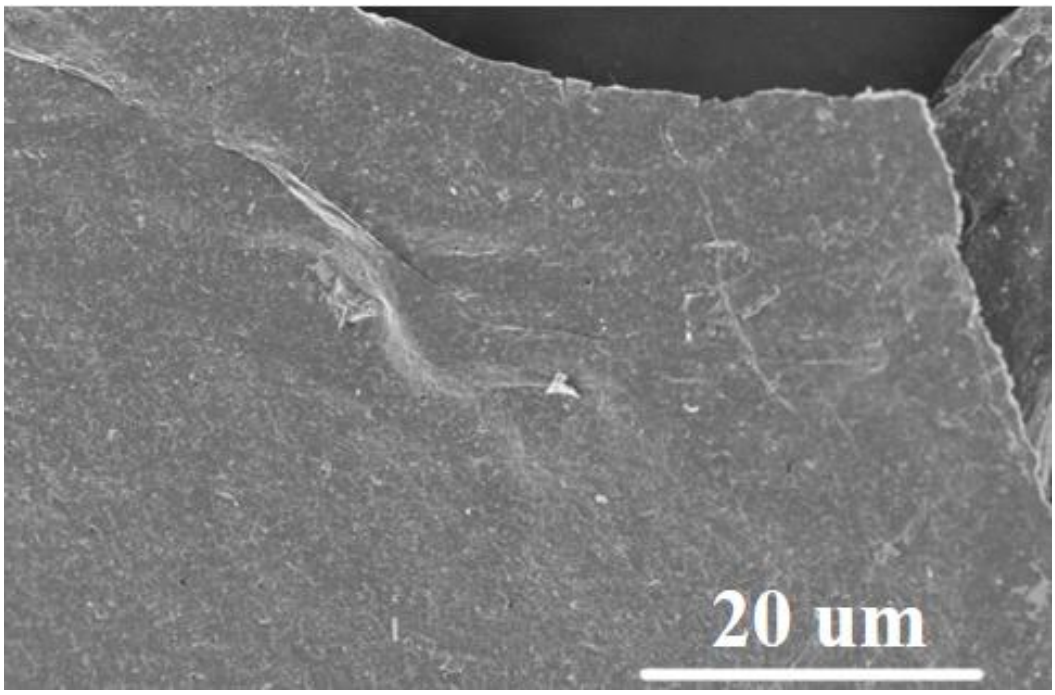

Fig. S7. SEM image of MXene after heat treatment at 600℃.

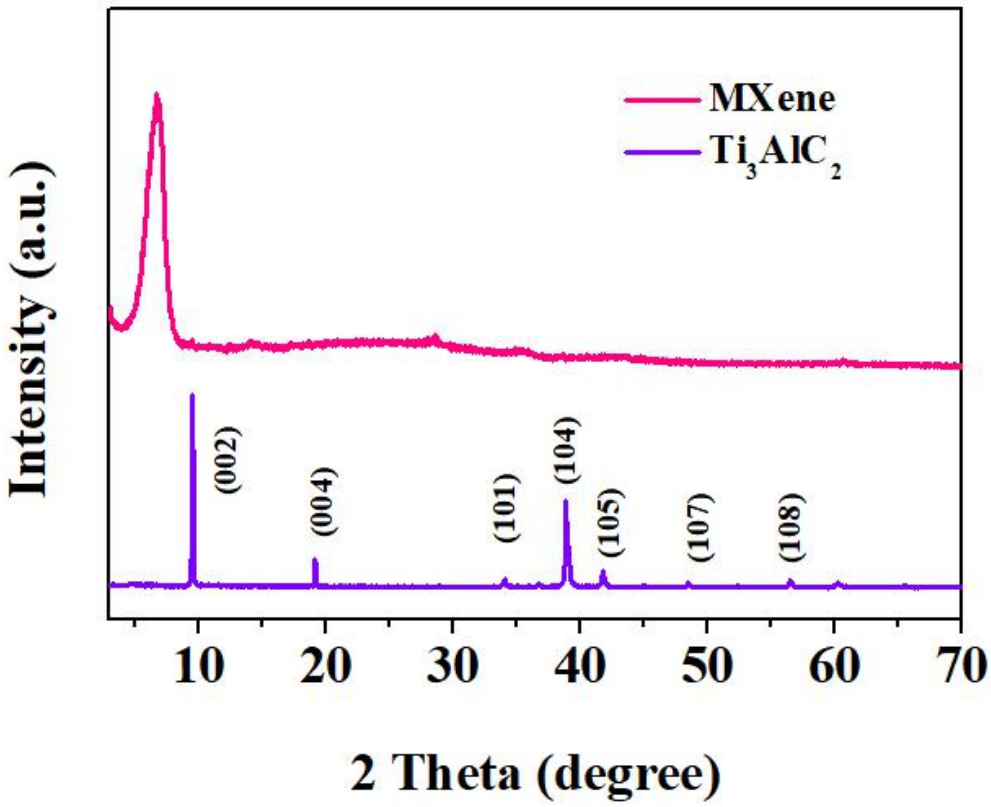

Fig. S8. XRD patterns of delaminated $Ti_3C_2T_x$ MXene and Ti_3AlC_2.

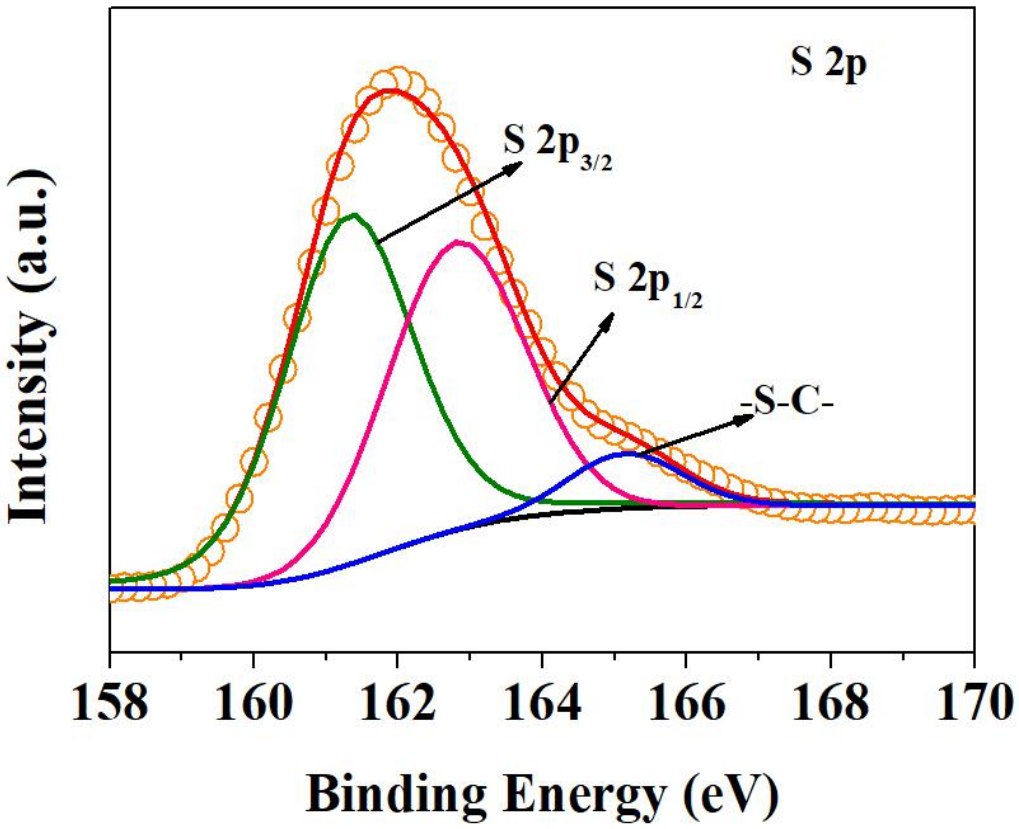

Fig. S9. High-resolution XPS spectra of S 2p for Co_9S_8 NP@NPC.

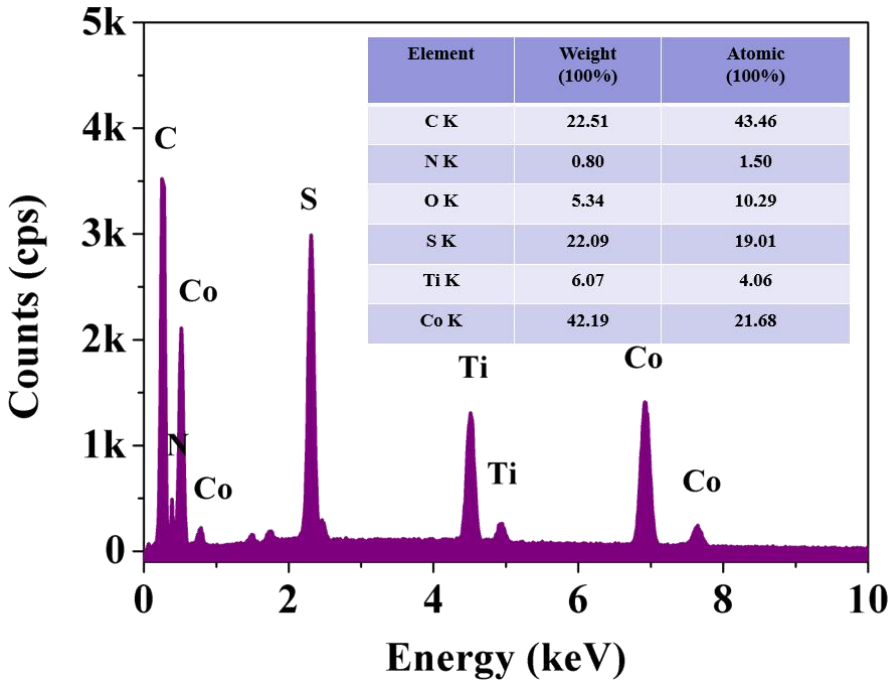

Fig. S10. Elemental analysis results from energy dispersive spectrometer in scanning electron microscopy (SEM-EDS) spectrum of Co_9S_8 NP@NPC@MXene.

Based on the atomic percentage of the carbon of MXene (Ti_3C_2) in the nanocomposite, the weight percentage of carbon of MXene (Ti_3C_2) could be calculated as follow:

$$C\ wt.\%\ of\ Ti_3C_2 = \frac{\text{molecular weight of C in MXene}}{\text{molecular weight of } Co_9S_8 \text{ QD@NPC@MXene}}$$

$$= \frac{12\times 2}{12\times 43.46 + 14\times 1.50 + 16\times 10.29 + 32\times 19.01 + 47.87\times 4.06 + 58.93\times 21.68}\times 100\% \approx 0.86\ \text{wt.\%}$$

$$Co_9S_8\ wt.\% = (Co + S)\ wt.\% = (42.19 + 22.09)\ wt.\% = 64.28\ wt.\%$$

$$MXene\ (Ti_3C_2)\ wt.\% = (Ti + C)\ wt.\% = (6.07 + 0.86)\ wt.\% = 6.93\ wt.\%$$

Thus, the carbon content of MXene (Ti_3C_2) is about 0.86 wt.%. Considering the carbon content of Co_9S_8 NP@NPC@MXene is about 22.51 wt.%, the carbon content of Co_9S_8 NP@NPC@MXene could be calculated as 21.65 wt.%. In addition, the content of Co_9S_8 is about 64.28 wt.% and the MXene is about 6.93 wt.%.

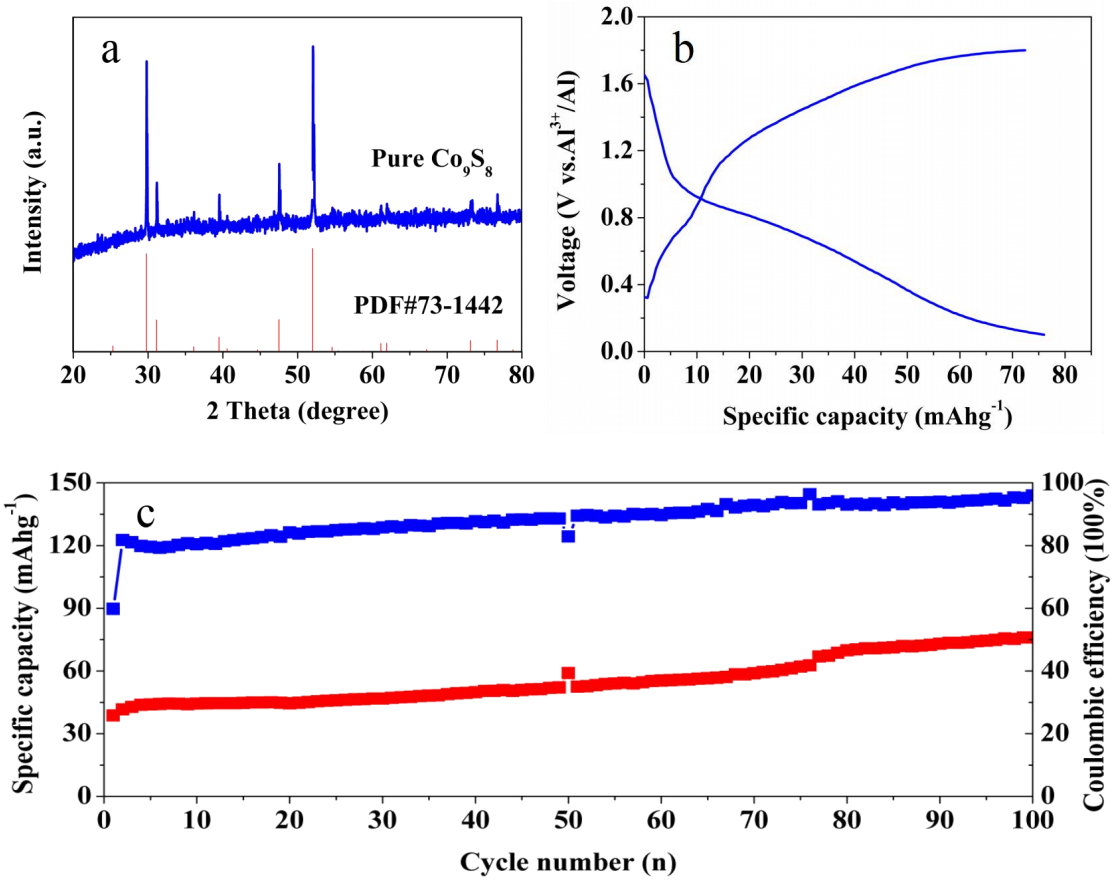

Fig.S11. (a) The XRD patterns of pure Co_9S_8 sample; (b) The GCD curve of bare Co_9S_8 cathode at 0.1 A g^{-1}; (c) The cycle stability of pure Co_9S_8 electrode at 0.2 A g^{-1}.

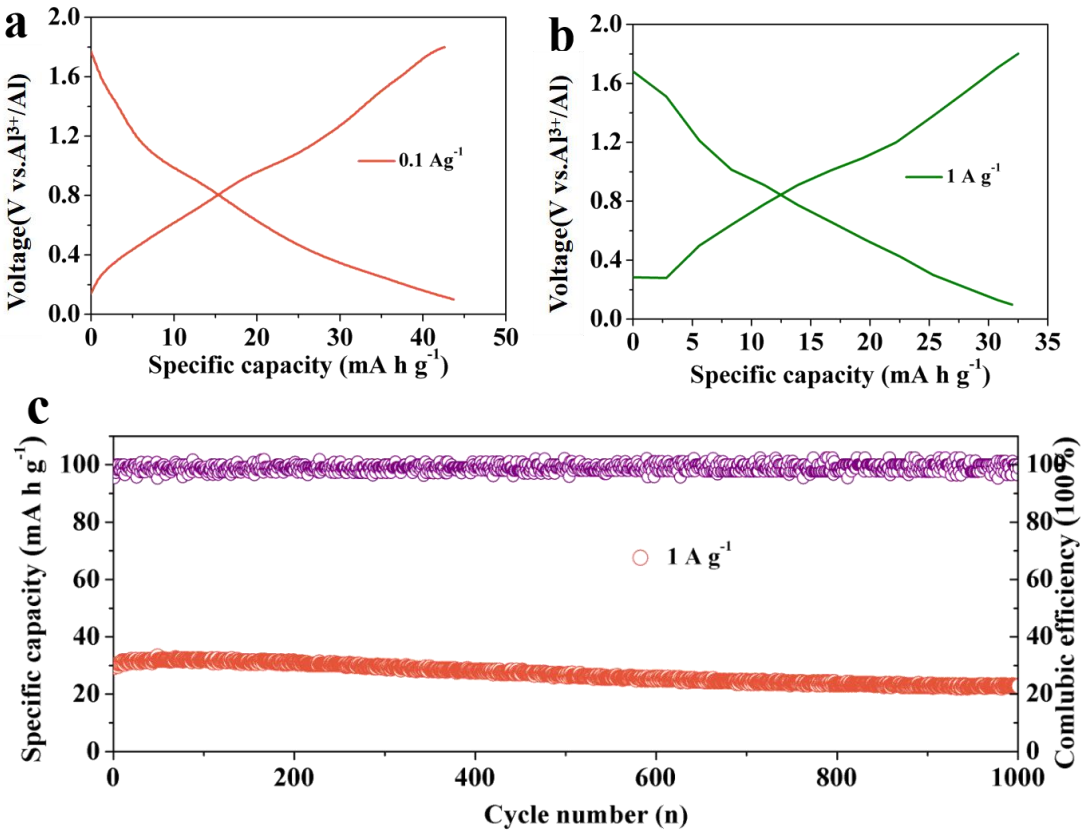

Fig. S12. (a)The GCD curves of MXene at 0.1 A g^{-1} and (b) 1 A g^{-1}.The long term cycling stability of MXene at 1 A g^{-1}.

It is noticed that the MXene delivered the specific capacities of about 45 mAh g^{-1} under 0.1 A g^{-1} current density. Considering the weight percent of the MXene (6.93%) in Co_9S_8 NP@NPC@MXene, about 3 mAh g^{-1} capacity was contributed by MXene, which is a negligible contribution to the Al ion storage.

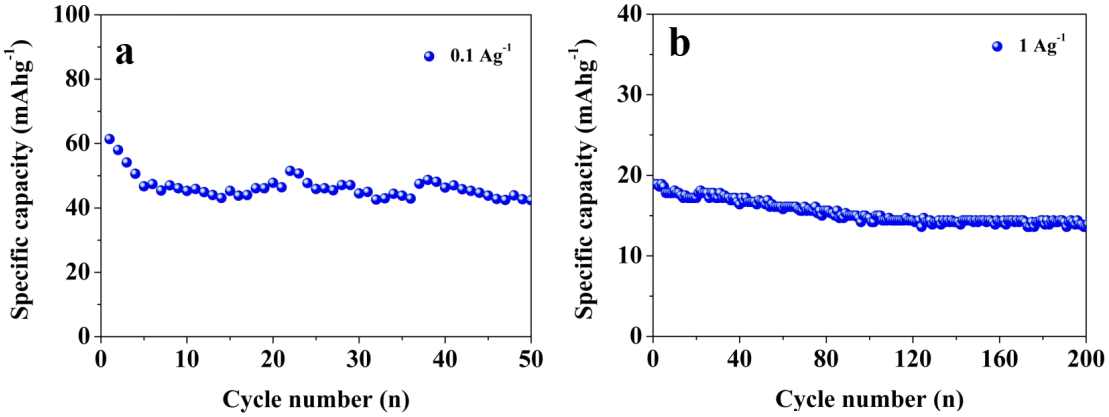

Fig. S13. (a) The cycle stability of ZIF-67 after high temperature treatment at 0.1 A g^{-1} (a) and 1 A g^{-1} (b).

It is noticed that the ZIF-67 after high-temperature treatment delivered the specific capacities of 60 mAh g^{-1} under 100 mAg^{-1} current density. Considering the weight percent of the carbon matrix (21.65%) in Co_9S_8 NP@NPC@MXene, about 13 mAh g^{-1} capacity was contributed by carbon, which is a negligible contribution to the Al ion storage. Therefore, the high capacity of the Co_9S_8 NP@NPC@MXene relied on the Co_9S_8 nanocrystals.

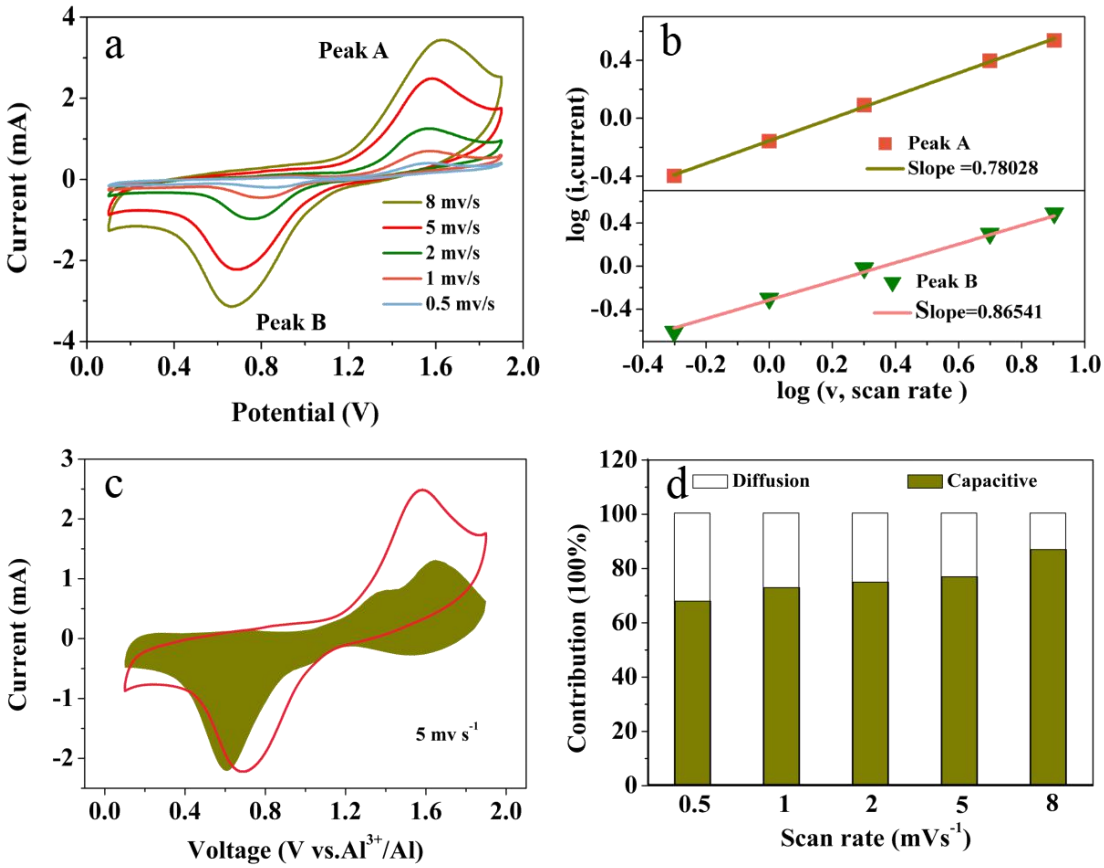

Fig. S14. CV curves from 0.5 to 8 mV s^{-1} of Co_9S_8 NP@NPC@MXene; (b) The log(i) versus log(v) plots at different CV peaks of Co_9S_8 NP@NPC@MXene; (c) Calculated capacitive contributions at 5 mV s^{-1} of Co_9S_8 NP@NPC@MXene; (d) A summary of capacitive contributions at different scan rates of Co_9S_8 NP@NPC@MXene.

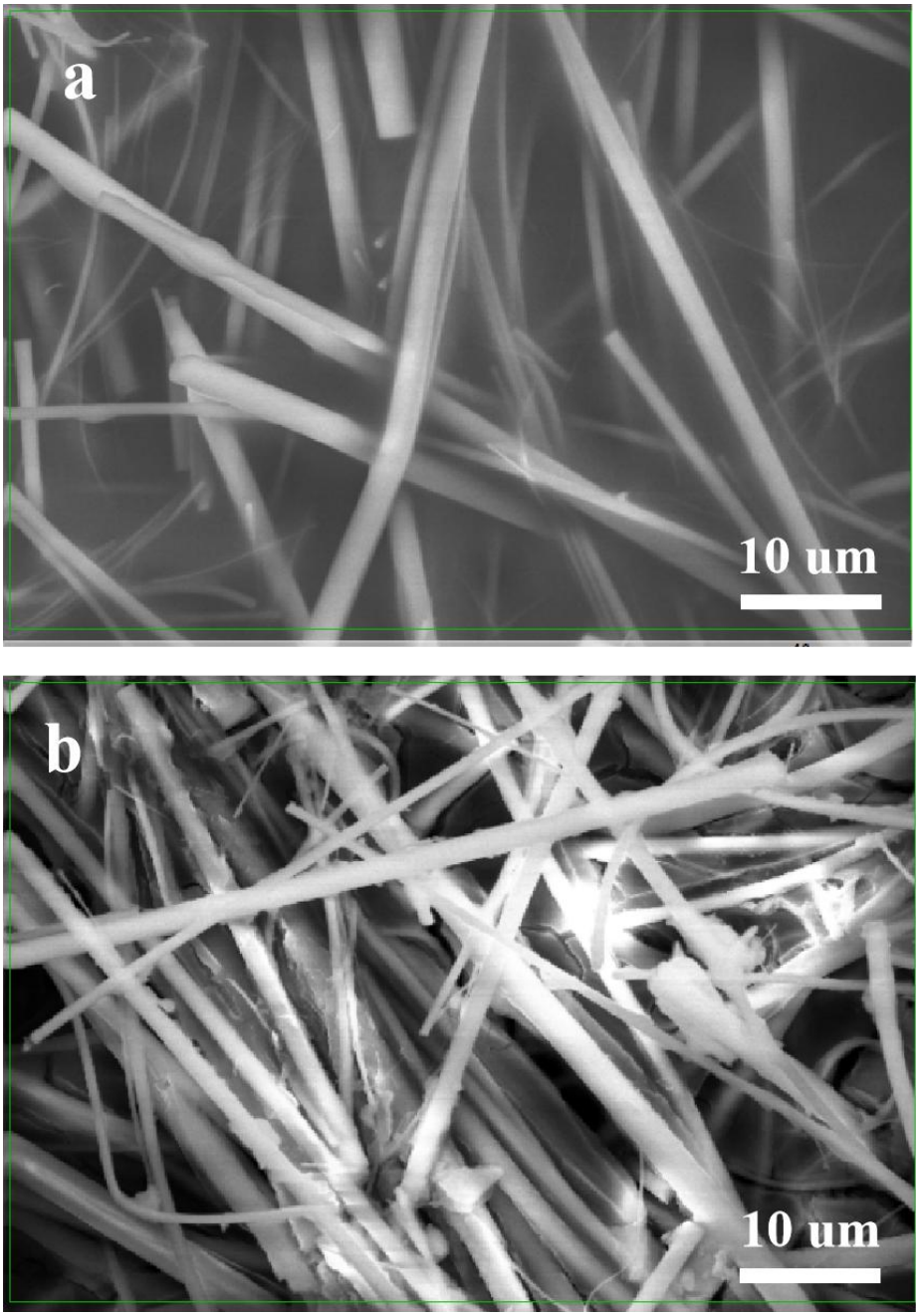

Fig. S15. The SEM images of the battery separator of the cell containing the (a) Co_9S_8 NP@NPC cathode and (b) Co_9S_8 NP@NPC@MXene cathode.

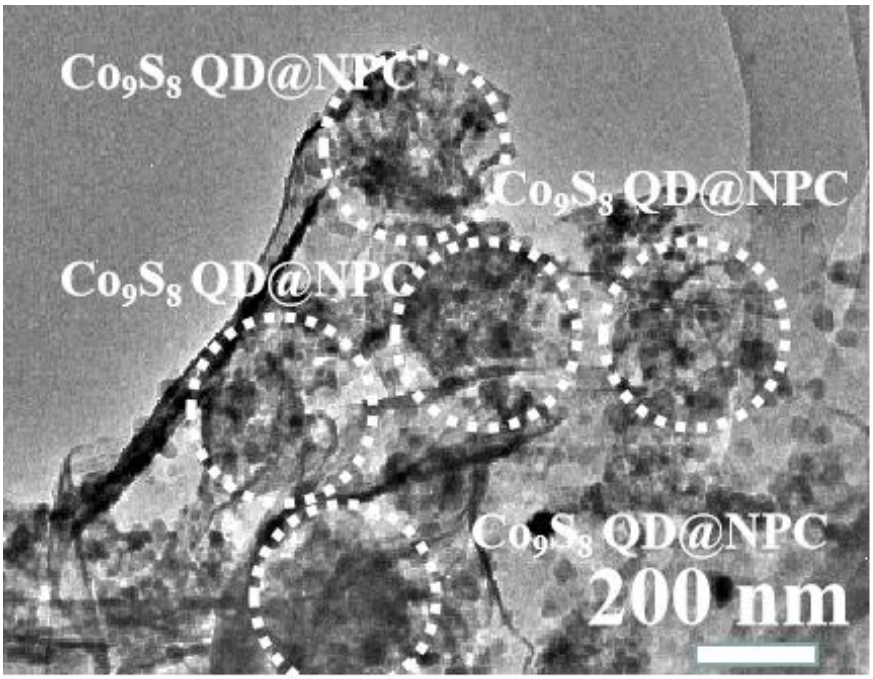

Fig. S16. The TEM image of Co_9S_8 NP@NPC@MXene cathode after 100 cycles.

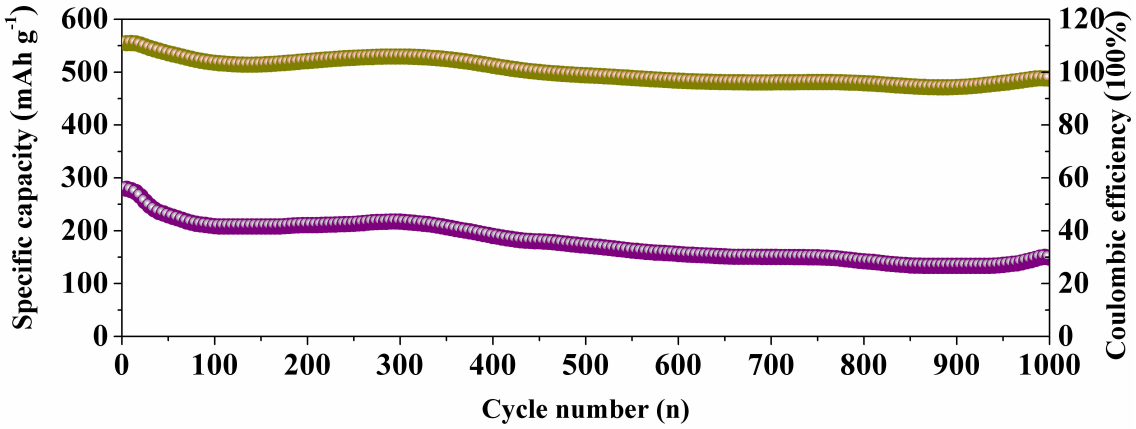

Fig. S17. The GCD curves of $CoSe_2$@NPC@MXene of the cell at different current densities.

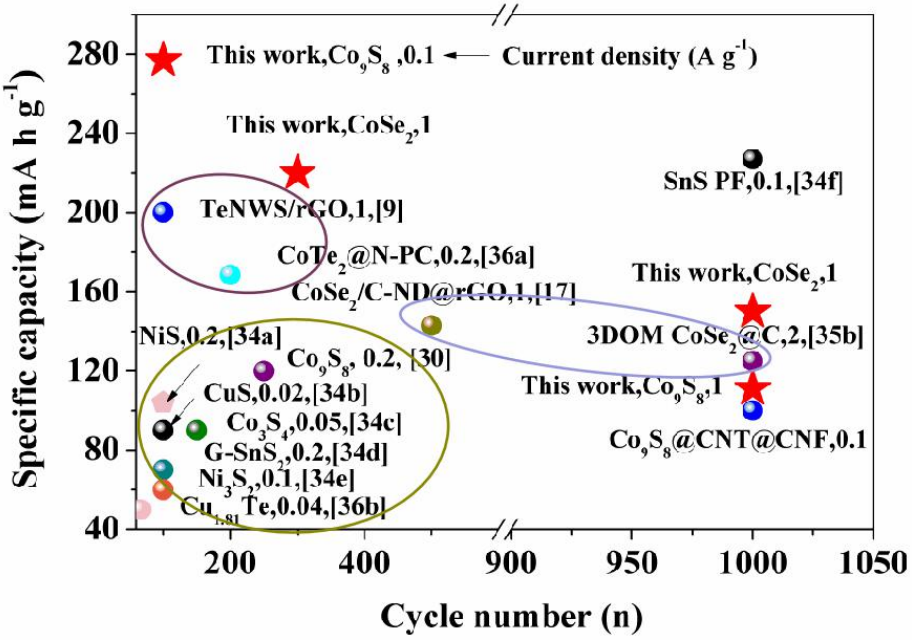

Fig. S18. Comparison of the performance of Co_9S_8 NP@NPC@MXene and $CoSe_2$@NPC @MXene electrode with most previously reported various types of RABs cathodes.

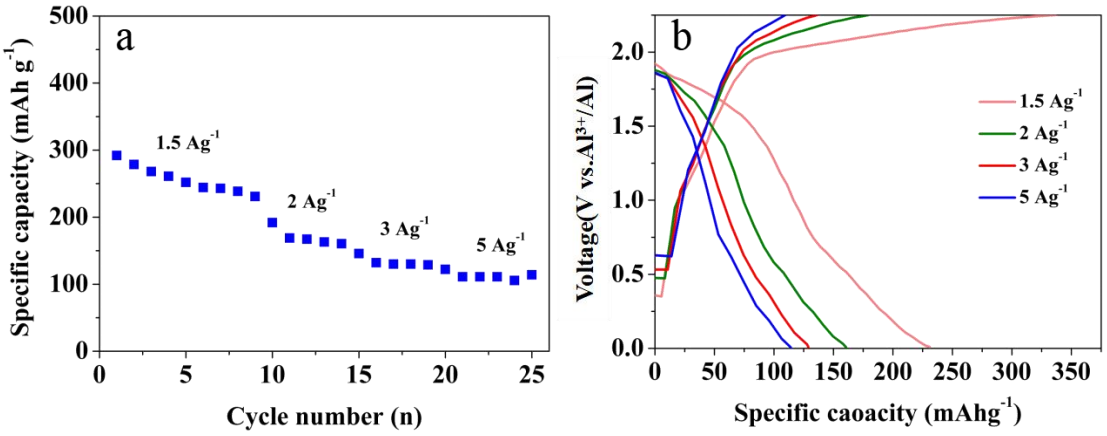

Fig. S19. The rate performance of $CoSe_2$@NPC@MXene (a), the GCD curves of different current densities (b).

Table S1. Comparison of electrochemical performance with the other representative metal sulfide cathode.

Sample	Current density ($A\ g^{-1}$)	Cycle number	Discharge capacity ($mA\ h\ g^{-1}$)	Ref.
Porous Co_9S_8	0.2	250	120	2
Co_9S_8@CNT-CNF	1	6000	87	3
Ni_3S_2@RGO	0.1	100	60	4
CuS@C	0.02	100	90	5
G-SnS_2	0.2	100	70	6
TiS_2	0.005	20	65	7
Co_3S_4	0.05	150	90	8
VS_2	0.1	50	50	9
MoS_2	0.04	100	66.7	10
VS_4@RGO	0.1	100	80	11
NiS	0.2	100	104	12
Co_9S_8NP@NPC@MXene	0.1	100	277	This work
	1	1000	110	

$CoSe_2$	1	300	220
@NPC@MXene	1	1000	150

References:

1 Y. Guo, Z. Hu, J. Wang, Z. Peng, J. Zhu, H. Ji, L.Wan, J. Angew. Chem. Int. Ed., 2020, 59, 22963-22967.

2 Z. Hu, K. Zhi, Q. Li, Z. Zhao, H. Liang, X. Liu, J. Huang, C. Zhang, H.Li, X.Guo, J. Power Sources, 2019, 440, 227147-227152.

3 Y. Hu, D. Ye, B. Luo, H. Hu, X. Zhu, S. Wang, L. Li, S. Peng, L. Wang, Adv. Mater., 2018, 30,1703824-1703829.

4 S.Wang, Z.Yu, J. Tu, J.Wang, D.Tian, Y. Liu, S. Jiao, Adv. Energy Mater., 2016, 13,1600137-1600146.

5 S.Wang, S.Jiao, J.Wang, H. S.Chen, D.Tian, H.Lei, D. N. Fang, ACS Nano, 2017,11, 469-477.

6 Y. Hu, B. Luo, D. Ye, X. Zhu, M. Lyu, L.Wang, Adv. Mater. 2017,29, 1606132-1606137.

7 L.Geng, J. P.Scheifers, C.Fu, J.Zhang, B. P. T.Fokwa, J.Guo, Titanium ACS Appl. Mater. Interfaces 2017,9, 21251-21257.

8 H. Li, H. Yang, Z. Sun, Y. Shi, H. M. Cheng, F. Li, Nano Energy 2019, 56, 100-108.

9 L. Wu, R. Sun, F.X iong, C. Pei, K.Han, C. Peng, Y. Fan, W.Yang, Q.An, L.Mai, Phys. Chem. Chem. Phys. 2018, 20, 22563-22568.

10 Z. Li, B. Niu, J. Liu, J. Li, F. Kang, ACS Appl. Mater. Interfaces, 2018,10, 9451-9459.

11 X. Zhang, S.Wang, J. Tu, G. Zhang, S. Li, D.Tian, S. Jiao, ChemSusChem, 2018,11, 709-715.

12 Z. Yu, Z. Kang, Z. Hu, J. Lu, Z. Zhou, S. Jiao, Chem. Commun. 2016, 52, 10427-10430.

13 X. Zhang, S. Jiao, J. Tu, W. L. Song, X. Xiao, S. Li, M. Wang, H. Lei, D.Tian, H.Chen, D. Fang, Energy Environ. Sci., 2019, 12, 1918-1927.

14 B. Zhang, Y. Zhang, J. Li, J. Liu, X. Huo, F. Kang, J. Mater. Chem. A, 2020, 8, 5535-5545.

15 K. Liang, L. Ju, S. Koul, A. Kushima, Y. Yang, Adv. Energy Mater., 2018, 9,1802543-1802549.

16 T. Cai, L. Zhao, H. Hu, T. Li, X. Li, S. Guo, Y. Li, Q. Xue, W. Xing, Z.Yan, L. Wang, Energy Environ. Sci. 2018,11, 2341-2347.

17 Y. Hu, D. Ye, B. Luo, H. Hu, X. Zhu, S. Wang, L. Li, S. Peng, L. Wang, Adv. Mater., 2018, 30, 1703824-1703829.

18 S.Wang, S. Jiao, J.Wang, H. S. Chen, D. Tian, H. Lei, D.N.Fang, ACS Nano, 2017,11, 469−477.

19 J. Wu, D.Wu, M.Zhao, Z. Wen, J. Jiang, J. Zeng, J. Zhao, Dalton Trans., 49 2020,49, 729-736.